Desalination and Water Treatment 320 (2024) 100615

Contents lists available at ScienceDirect

Desalination and Water Treatment

journal homepage: www.sciencedirect.com/journal/desalination-and-water-treatment/

Electrochemical treatment of azo dye wastewater by dynamic flow diaphragm system: Response surface methodology optimization and energy consumption analysis

Ao Xiao*,[1], Fuchen Ban, Xiaoyi Tong, Chenjian Ye, Yu Wei

School of Municipal and environmental engineering, Shenyang Jianzhu University, Shenyang, China

ARTICLE INFO

Keywords:
Amaranth red
Diaphragm system
Electrochemical oxidation
Response surface method

ABSTRACT

In this experiment, the degradation process of azo dye wastewater was studied based on the diaphragm double chamber electrochemical reactor, taking the mono azo dye amaranth as an example. Through the circulation flow of appropriate volume of wastewater in the cathode and anode chamber, the simultaneous action of cathode and anode was realized, and the degradation and decolorization efficiency of azo wastewater was improved while reducing energy waste. The optimal reaction conditions optimized by response surface methodology were as follows: the voltage was 20.74 V, the plate spacing was 4.89 cm, and the cycle speed was 60.66 rad / min. The optimal decolorization rate was 99.66 %. The energy consumption analysis of the dynamic flow diaphragm system electrochemical method and the static flow diaphragm system electrochemical method for the treatment of azo dye wastewater was compared and analyzed. In addition, the possible degradation process of azo dye wastewater by dynamic flow electrochemistry was inferred by ultraviolet spectroscopy and mechanism prediction analysis. The experimental results show the great potential of the dynamic flow membrane system process in the treatment of azo dyes.

1. Introduction

Synthetic dyes are widely used in the textile and printing industry. They are often discharged into the environment and cause environmental pollution[1]. Azo dyes, containing at least one azo group (-N = N-) as a chromophore and other functional groups, account for about 70 % of the annual global dye production [2]. Azo dyes are highly stable under light and are not easily degraded by microorganisms [3]. The emission of azo dyes and their toxic, mutagenic and persistent by-products can lead to serious environmental problems [4]. Therefore, azo dye wastewater must be treated before it is finally discharged into the environment. Some advanced oxidation methods can effectively degrade dye wastewater, such as Fenton method [5], photocatalytic oxidation method [6,7], ozone oxidation method [8,9] can effectively remove dyes, but there are problems such as high cost and difficult control of reaction conditions.

Electrochemical advanced oxidation processes (EAOPs) have attracted great attention in the degradation of refractory organic pollutants. The technology mainly uses the active groups such as·OH, H_2O_2 and superoxide radical ($\cdot O_2$) produced by electrolysis on the electrode surface to indirectly oxidize the organic pollutants in the wastewater, and finally completely degrade them into harmless small molecules such as CO_2 and H_2O [10]. Cotillas et al. [11]used stainless steel as cathode and boron-doped diamond electrode (BDD) as anode, and used electrocatalytic oxidation to decolorize and degrade reactive red dye. After 240 min electrolysis reaction, both chroma and COD can be completely removed , and the treatment effect reaches 100 %. Jiao et al. [12]used a flow reactor to treat acid orange II dye wastewater by electro-Fenton process with carbon black and polytetrafluoroethylene modified activated carbon fiber as cathode. The decolorization rate reached 96.7 % and the mineralization efficiency reached 55.4 % when the reaction was carried out for 120 min

However, in the process of electrochemical reaction, the cathode and anode plates are subjected to redox reactions respectively, which will interfere with each other and affect the progress of the reaction. Therefore, some researchers put forward the concept of diaphragm system [13–17]. Hu et al. [18] designed an iron rod cathode, BBD double anode electrolyzer, and used nafion proton exchange membrane

* Corresponding author.
E-mail address: xa12340222@163.com (A. Xiao).
[1] First author

https://doi.org/10.1016/j.dwt.2024.100615
Received 1 April 2024; Received in revised form 12 July 2024; Accepted 12 July 2024
1944-3986/© 2024 The Author(s). Published by Elsevier Inc. This is an open access article under the CC BY-NC-ND license (http://creativecommons.org/licenses/by-nc-nd/4.0/).

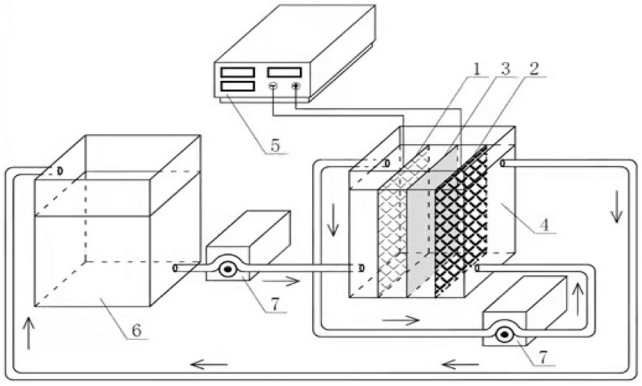

Fig. 1. Device schematic(1.Cathode; 2. Anode; 3.Proton exchange membrane; 4.Reaction tank; 5. Power supply; 6.Reservoir; 7. peristaltic pump).

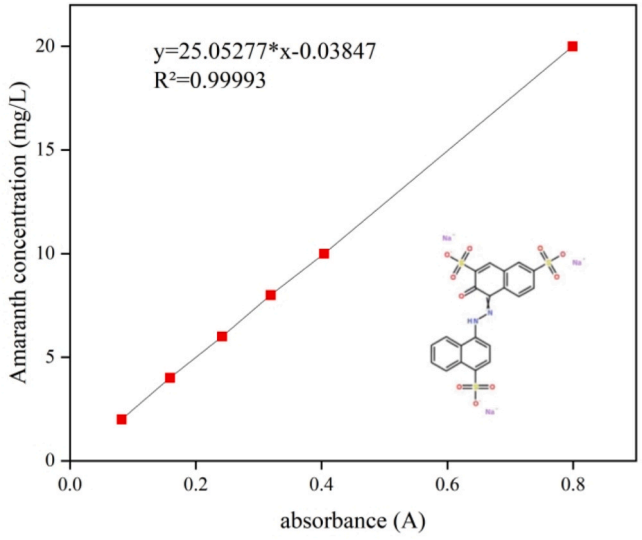

Fig. 2. The standard curve of absorbency-concentration.

Table 1
Coding and level design factors.

Factors	variable	level		
		-1	0	1
Voltag (V)	A	15	20	25
Plate spacing(cm)	B	4	5	6
Circulation speed (rad/min)	C	50	60	70

as a separator. The removal rate of dichlorophenol exceeded 99 %, showing excellent removal effect. However, there are still some defects in the membrane system, such as the relatively low degradation efficiency of pollutants in the cathode chamber, the deposition and accumulation of pollutants in the cathode chamber.

In this experiment, a diaphragm double-chamber electrochemical reactor was used to study the degradation process of azo dye wastewater. The diaphragm material divided the electrolytic cell into two anode and cathode chambers. The titanium plate was used as the cathode and the ruthenium-iridium-coated titanium electrode was used as the anode. Through the circulation flow, the cathode and anode were simultaneously operated to reduce the energy waste and improve the degradation and decolorization efficiency of azo wastewater. In the experiment, the Box-Behnken Design (BBD) Response Surface Method (RSM)was used to study the optimal treatment conditions and the interaction of different factors, and the static flow diaphragm system electrochemical method and the dynamic flow diaphragm system electrochemical method were compared and analyzed from the aspect of energy consumption, so as to further verify the superiority of the dynamic flow diaphragm system.

2. Materials and methods

2.1. Materials

As shown in Fig. 1, the reactor device is mainly composed of a DC regulated power supply, a peristaltic pump, an electrolytic cell, an electrode plate, a diaphragm. The material of the electrolytic cell is organic glass, the size is 10 cm × 10 cm × 10 cm, and the effective volume is 800 mL. In the plate, the anode is ruthenium iridium coated titanium electrode and graphite felt electrode, and the cathode is stainless steel electrode and titanium electrode. The effective area of the plate is 5 cm × 10 cm, which is purchased from Suzhou Shuertai Industrial Technology Co., Ltd.; the proton exchange membrane Nafion-117 with an effective area of 5 cm × 5 cm was purchased from Suzhou Shengernuo Technology Co., Ltd. Digital distribution peristaltic pump (YZ1515X type), purchased from Baoding Chuangrui Pump Co., Ltd.; dC regulated power supply (YJ34 type), purchased from the Great Wall Electrical Instrument Factory; ultraviolet-visible spectrophotometers (WFJ2100 and 8453) were purchased from Shanghai Unocal Instrument Co., Ltd.and Agilent, USA.

2.2. Methods

2.2.1. Plate and diaphragm pretreatment

The electrode plate was immersed in dilute sulfuric acid for 24 h, and then washed with deionized water to remove surface impurities and organic matter, and then immersed in deionized water for 12 h, and dried in a 110 °C drying oven.

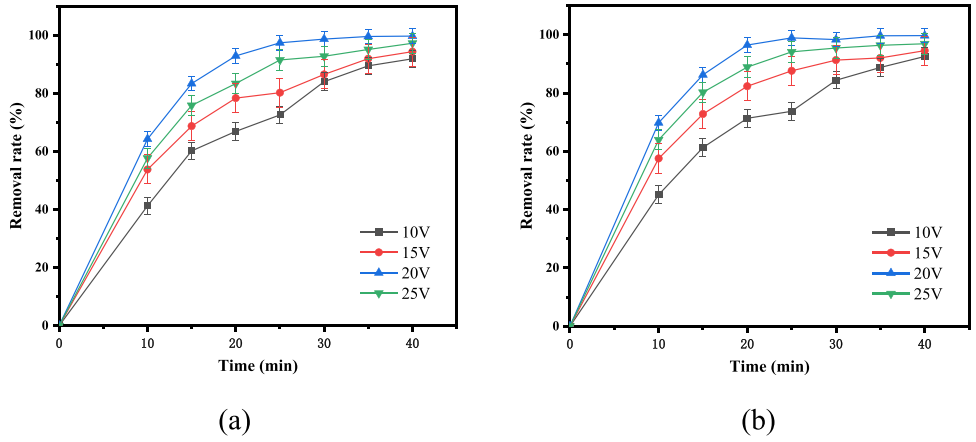

Fig. 3. Effect of the voltage on the Amaranth red removal rate at cathode (a) and anode (b).

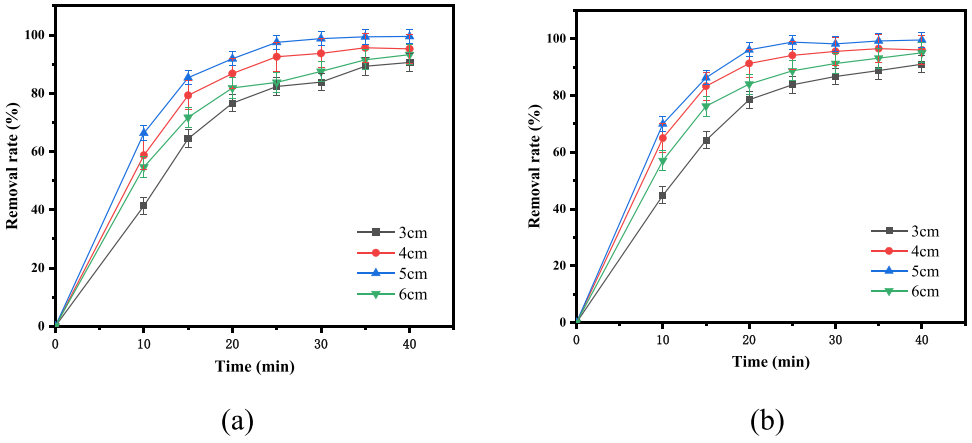

Fig. 4. Effect of the plate spacing on the Amaranth red removal rate at cathode (a) and anode (b).

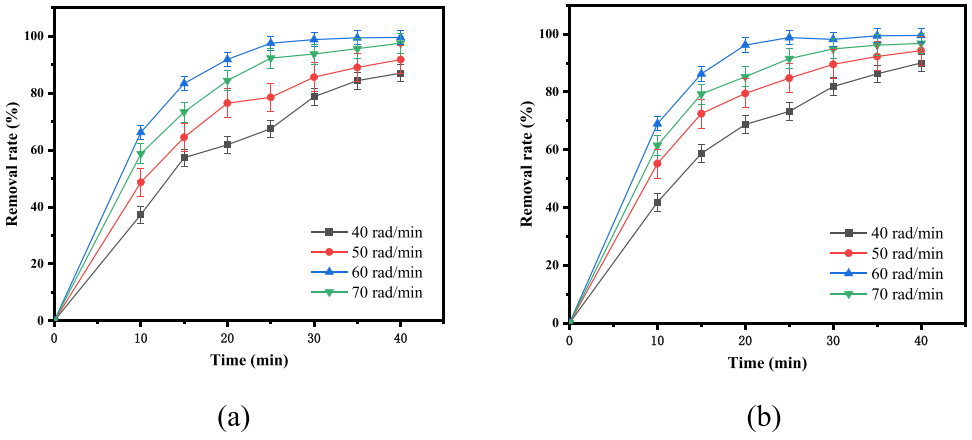

Fig. 5. Effect of the cycling speed on the Amaranth red removal rate at cathode (a) and anode (b).

Table 2
Response Surface Experimental Design and Results.

serial number	voltage (V)	plate spacing (cm)	circulation velocity (rad/min)	decolorization rate (%)
1	20	6	50	89.72
2	20	5	60	99.74
3	15	5	50	89.28
4	20	5	60	99.73
5	15	5	70	90.53
6	15	4	60	91.24
7	20	4	50	91.18
8	20	5	60	98.97
9	20	5	60	99.44
10	25	6	60	92.47
11	15	6	60	92.15
12	25	5	50	91.27
13	20	6	70	90.68
14	20	4	70	92.78
15	25	4	60	94.58
16	25	5	70	92.62
17	20	5	60	99.82

The membrane was treated with 5 % hydrogen peroxide at 80 ˚C for 1 h, and then immersed in deionized water for half an hour. Then it was boiled with 5 % dilute sulfuric acid at 80 ˚C for 1 h. Finally, it was boiled in deionized water at 80 ˚C for 30 min

2.2.2. Electrochemical oxidation of a dynamic flow membrane system

Before the start of the experiment, all switches and valves were closed, and a certain concentration of azo dye simulated wastewater was added to the electrolytic cell, and then the electrolyte was added and stirred until it was completely dissolved. The pretreated electrode plate and diaphragm material are installed in the electrolytic cell, and the power supply is pre-connected and the valve on both sides of the electrolytic cell is connected with a hose to prepare for the liquid circulation in the cathode and anode chambers. After the preparation work is completed, start the peristaltic pump. When the bubbles in the rubber tube flow uniformly, it can be regarded as the dynamic cycle of the diaphragm system. Finally, the power supply is started to electrolyze the azo dye wastewater.

2.2.3. Determination of standard absorption curve of amaranth

As shown in Fig. 2, the standard absorption curve of amaranth was measured and plotted, and the decolorization removal rate was calculated as follows:

$$\eta = \frac{A_0 - A_t}{A_0} \times 100\% \quad (1)$$

In the equation: η is the removal rate of decolorization, $A_0$is the absorbance of the solution before treatment, A_t is the absorbance of the solution at time t.

2.2.4. Response surface analysis

In this study, BBD response surface method was used to optimize the experimental conditions for the treatment of azo wastewater by dynamic membrane electrochemical system. The response surface method is a combination of statistics and mathematics [19]. This method can use the data to draw the response surface diagram, and obtain the global real optimal operating point by analyzing the model. Compared with the complete factor level design and CCD response surface

Table 3
Response Surface Experimental Design and Results.

item	quadratic sum	degree of freedom	square	F ratio	P ratio (Prob > F)	-
Mean vs Total	1.499	1	1.499			
Linear vs Mean	13.65	3	4.55	0.2503	0.8597	
2FI vs Linear	2.39	3	0.7950	0.0340	0.9911	
Quadratic vs 2FI	232.69	3	77.56	449.51	< 0.0001	Suggested
Cubic vs Quadratic	0.7185	3	0.2395	1.96	0.2624	Aliased
Residual	0.4894	4	0.1223			
Total	1.501	17	8830.81			

Table 4
ANOVA results of the regression model R1(Removal rate of amaranth).

Std. Dev.	0.4154	R^2	0.9952
Mean	93.89	Adjusted R^2	0.9890
C.V.%	0.4424	Predicted R^2	0.9509
		Adeq Precision	32.0239

method, the BBD response experiment has fewer test times and lower cost. In this study, several factors that have a great influence on amaranth dye were selected, namely voltage, plate spacing and cycle speed, which were recorded as variables A, B and C. The value range of each variable is voltage 15 ~ 25 V, plate spacing 4 ~ 6 cm, cycle speed 50 ~ 70 rad/min, and the response value is the single azo dye amaranth cathode chromaticity rate (Y). The BBD model in Design Expert 11 software was used to design a three-factor and three-level test plan. Design factors and levels are shown in Table 1. Through software simulation modeling, the corresponding optimal reaction conditions were finally fitted.

2.2.5. Ultraviolet-visible absorption spectroscopy and LC-MS analysis

The water samples in the electrolytic cell with reaction time of 0, 10, 20, 30, 40 min were selected and scanned by UV–visible absorption spectrum [20]. The wavelength was set between 200 and 900 nm. The experimental data were analyzed and the UV–vis spectrogram was generated. By observing and comparing the peak value and the changes before and after, the structural change process and reaction path in the process of pollutant removal were inferred.

In the LC-MS analysis, the following parameters were used: mobile phase A was 0.1 % formic acid water, mobile phase B was acetonitrile solution. The flow rate was set to 0.2 mL / min, and the single injection volume was 1 μL. The chromatographic column was Waters BEH C18, the size was 2.1 × 100 mm, the particle size was 1.7 μm, and the column temperature was 40 °C. The mass spectrometry scanning range was set from 50 to 500 m / z. In ESI-mode, the voltage is set to 3500 V.

3. Result and discussion

3.1. Single factor analysis

3.1.1. Effect of voltage

The amaranth dye was tested at 10–25 V voltage. As shown in Fig. 3, it can be seen that within a certain range, with the increase of voltage, the degradation and decolorization effect of the dynamic flow membrane system on amaranth dye is improved. When the reaction time is 40 min and the reaction voltage is 20 V, the degradation effect of amaranth is the best, and the decolorization rate in the anode and cathode chambers reaches 99.54 %. When the voltage increases from 10 V to 20 V, the decolorization effect increases significantly, which indicates that the electric field effect increases with the increase of voltage. Under the condition of keeping the plate spacing unchanged, the current and electron transfer rate are increased, so that the oxidation of organic matter produced by the cathode and anode is increased, and the effect of degradation and removal of azo dyes is improved [21]. However, when the voltage is further increased to 25 V, the decolorization rate of azo dyes does not increase but decreases. Because as the voltage increases, although it promotes the reaction of degrading organic matter, a large number of bubbles are generated on the electrode surface, the active area on the electrode surface will be reduced, and the service life of the electrode plate will also be affected. Therefore, although some scholars believe that higher voltage will have better synchronization effect, the use of less electrical energy in this experiment can also achieve the best results [22]. Therefore, 20 V is finally selected.

as the reaction voltage.

3.1.2. Effect of plate spacing

The amaranth dye was tested by adjusting the plate spacing to 3, 4, 5 and 6 cm, respectively. As shown in Fig. 4 that the removal rate of amaranth dye by the dynamic flow separator system increases first and then decreases with the increase of plate spacing. When the reaction time was 40 min, the plate spacing increased from 3 cm to 5 cm, and the

Table 5
Evaluation of the regression model R1.

item	The sum of variance	degree of freedom	mean square deviation	F ratio	Adjoint probability P value	-
Model	248.72	9	27.64	160.16	< 0.0001	significant
A-voltage	7.49	1	7.49	43.40	0.0003	
B-plate spacing	2.83	1	2.83	16.41	0.0049	
C-cycling speed	3.33	1	3.33	19.29	0.0032	
AB	2.28	1	2.28	13.21	0.0083	
AC	0.0025	1	0.0025	0.0145	0.9076	
BC	0.1024	1	0.1024	0.5935	0.4663	
A^2	52.99	1	52.99	307.09	< 0.0001	
B^2	48.17	1	48.17	279.19	< 0.0001	
C^2	108.12	1	108.12	626.63	< 0.0001	
Residual	1.21	7	0.1726			
Lack of Fit	0.7185	3	0.2395	1.96	0.2624	not significant
Pure Error	0.4894	4	0.1223			
Cor Total	249.93	16				

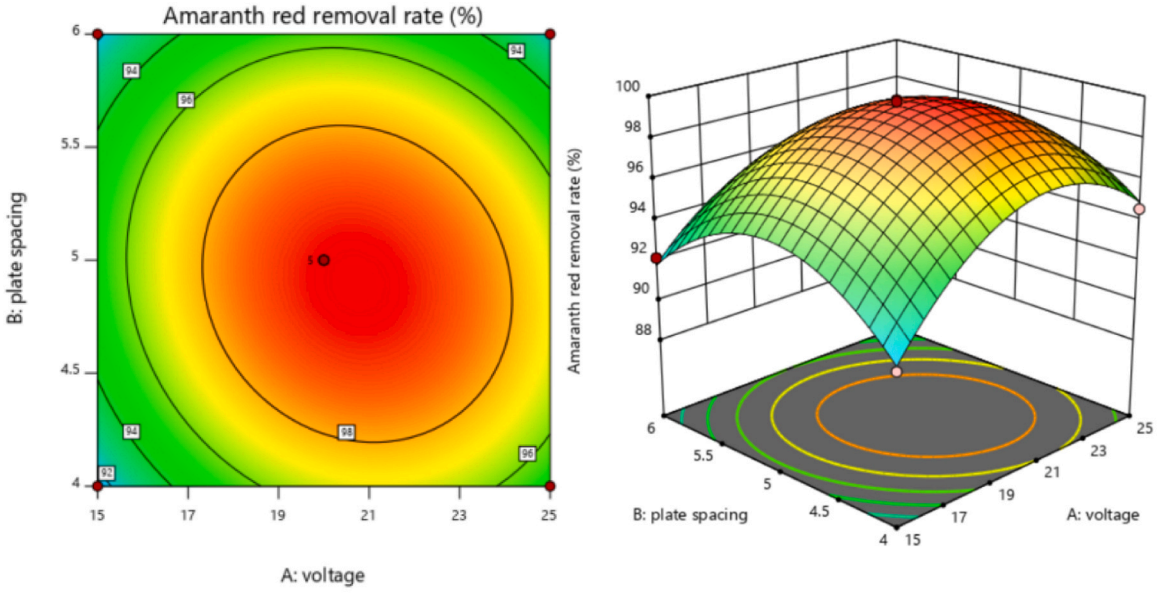

Fig. 6. Contour diagram (la) and response surface diagram (b) of the voltage and the plate spacing interaction.

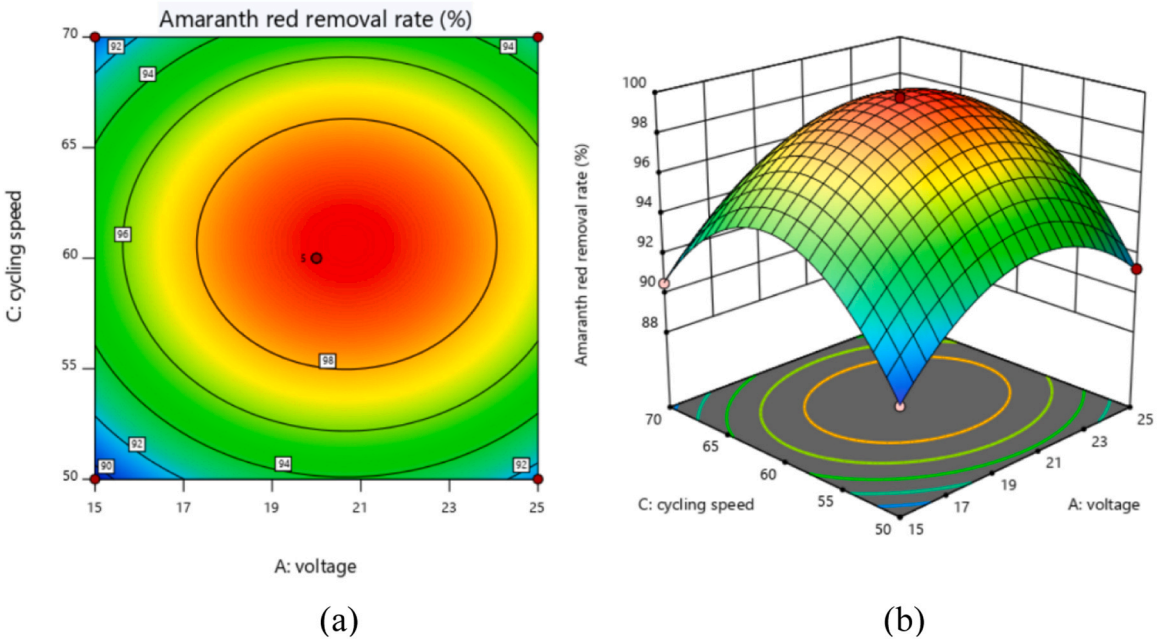

Fig. 7. Contour diagram (a) and response surface diagram (b) of the voltage and the cycling speed interaction.

decolorization rate of amaranth dye increased from 90.52 % and 91.02 % to 99.54 %, respectively. When the plate spacing is small, the reaction space between the two plates is also small, that is, the space for efficient removal of organic matter is small; at the same time, the smaller plate spacing will also cause the current and resistance to increase, resulting in a serious concentration polarization phenomenon, making the current efficiency low, affecting the decolorization efficiency of the dye. Therefore, increasing the plate spacing is beneficial to the removal of organic matter.

However, with the further increase of the plate spacing, the color removal rate of amaranth dye in the cathode and anode chambers decreased to 93.27 % and 95.03 %, indicating that when the plate spacing increased to a certain extent, the mass transfer distance between electrons and effective active substances increased, and the resistance of the whole system increased, the electric field intensity decrease, which would affect the efficient degradation of organic matter [23]. At the same time, the number of active substances effectively participating in the reaction per unit volume will be reduced [24], resulting in the decrease of chromaticity and degradation efficiency at the same time. Therefore, the plate spacing is selected as 5 cm for the experiment.

3.1.3. Effect of Cycle speed

The amaranth dye was tested by controlling the circulation speed of 40,50,60,70 rad/min. As shown in Fig. 5, when the cycle speed increases from 40 rad/min to 60 rad/min, the removal rate of amaranth dye increases continuously, and the removal rate of amaranth dye in the cathode chamber increases from 87.00 % to 99.54 %. When the cycle speed continues to rise, the removal rate in the cathode chamber decreases to

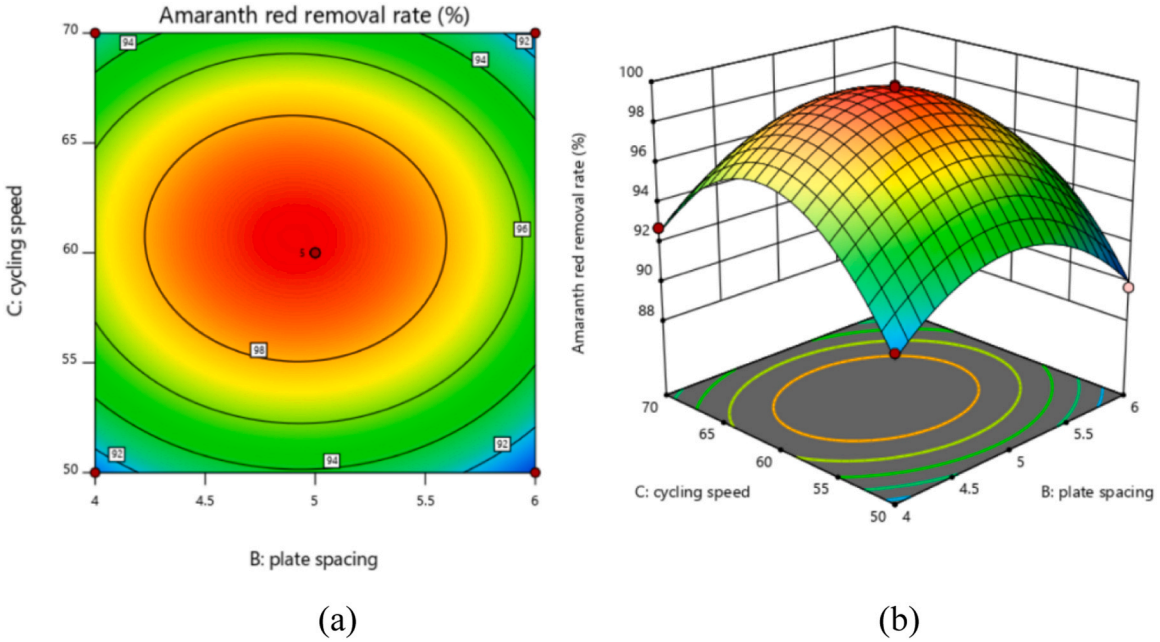

Fig. 8. Contour diagram (a) and response surface diagram (b) of the plate spacing and the cycling speed interaction.

Table 6
The current value and decolorization rate of different voltage in static diaphragm system.

Voltage U (V)	Electricity I (A)	Anode decolorization rateE_1 (%)	Cathodic decolorization rateE_2 (%)
5	0.43	77.18	34.03
7.5	0.54	82.54	38.17
10	0.62	86.36	42.92
12.5	0.71	92.35	46.59
15	0.79	96.84	50.03

Table 7
the current value and decolorization rate of different voltage in circulating diaphragm system.

Voltage U (V)	Electricity I (A)	Anode decolorization rate E_3 (%)	Cathodic decolorization rate E_4 (%)
5	0.48	71.12	68.73
7.5	0.63	76.74	74.67
10	0.78	83.52	80.02
12.5	0.89	89.76	86.46
15	1.02	95.53	93.28

97.53 %. On the one hand, the purpose of dynamic flow is to use the anode to destroy the nitrogen-nitrogen double bond, form nitroaromatic compounds, and then reduce them to amine and hydroxyl aromatic compounds which are more conducive to oxidation through cyclic flow to the cathode, so as to accelerate the reaction and make efficient use of the cathode. On the other hand, some air is introduced into the circulation process to provide oxygen for the reaction, which can also increase the agitation and reduce the current short circuit in the solution. Therefore, with the increase of the cycle speed, the cycle mass transfer process is also accelerated, and the decolorization effect of azo dye is improved. However, if the circulation speed is too fast, the effective reaction in the cathode and anode chamber will be incomplete, and the effect of cathode and anode synchronization cannot be achieved, but the processing efficiency will be reduced.

3.2. Box-Behnken design Response surface analysis

3.2.1. BBD scheme design

According to the requirements of response surface design, 17 experiments were carried out. The specific response surface design is shown in Table 2.

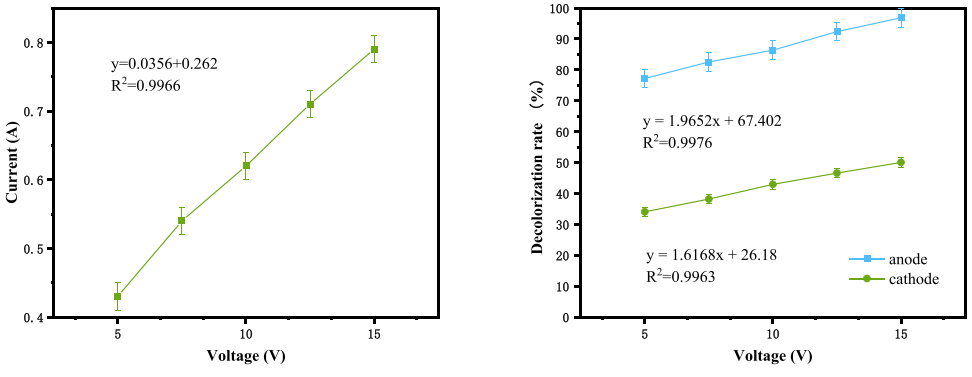

Fig. 9. Relationship between voltage and current (a)、relationship between the voltage and the decolorization rate (b) in static diaphragm system.

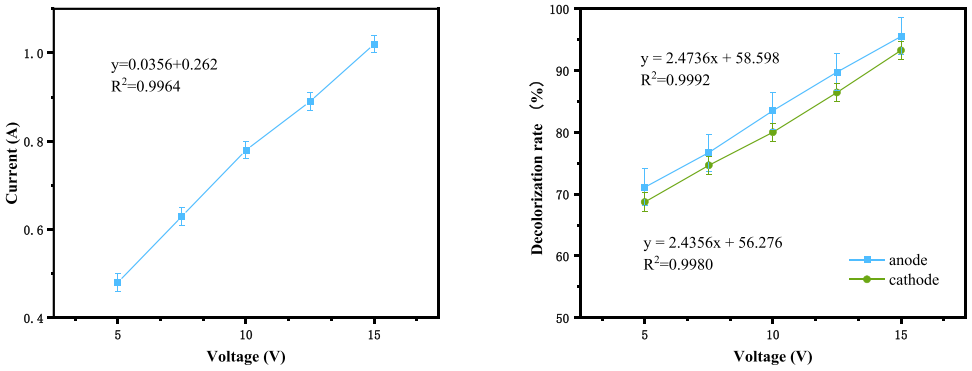

Fig. 10. Relationship between voltage and current (a)、voltage and the decolorization rate (b) in circulating diaphragm system.

Table 8
The relationship between the decolorization rate of amaranth red and energy consumption of the static diaphragm and the circulating diaphragm system.

decolorization rateE (%)	W_1 (kW·h)	W_2 (kW·h)	W_3 (kW·h)	W_4 (kW·h)	$W_1 + W_2$ (kW·h)	$W_3 + W_4$ (kW·h)	$W_3 + W_4/W_1 + W_2$
0	32.89	5.09	24.77	23.44	37.98	48.21	1.27
10	22.72	0.94	16.29	15.09	23.66	31.38	1.33
20	14.39	0.49	9.57	8.54	14.88	18.11	1.22
30	7.89	0.80	4.61	3.79	8.69	8.40	0.97
40	3.24	4.81	1.41	0.84	8.05	2.25	0.28
50	0.43	11.54	0.03	0.30	11.97	0.33	0.03
60	0.05	20.99	0.29	0.34	21.04	0.63	0.03
70	0.32	33.16	2.37	2.79	33.48	5.16	0.15
80	3.03	48.05	6.21	7.04	51.08	13.24	0.26
90	7.57	65.66	11.80	13.09	73.24	24.89	0.34
100	13.96	85.99	19.16	20.94	99.95	40.10	0.40

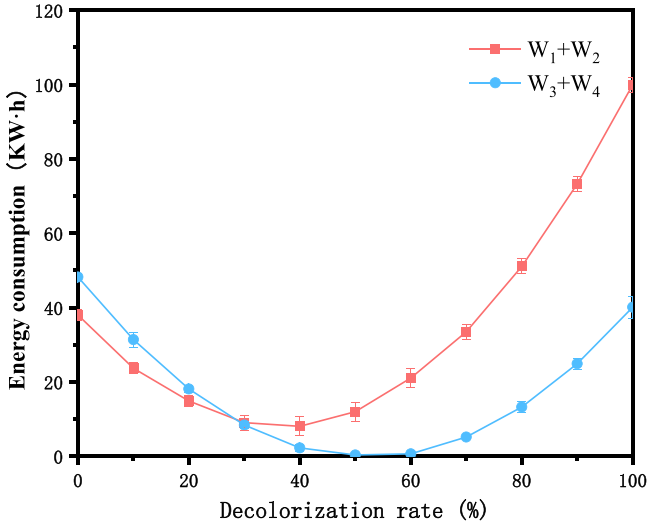

Fig. 11. Energy comparison between the static diaphragm and the circulating diaphragm.

3.2.2. Model establishment and optimization analysis

The design of BBD includes a variety of polynomial responses, such as linear polynomial response (Linear), quadratic polynomial response (Quadratic), cubic polynomial response (Cubic), and two-factor interaction polynomial response (2FI). The polynomial type that is most suitable for the test is selected by analyzing the results. The specific results are shown in Table 3.

According to the results of Table 3, when $P < 0.0001$, it shows that the model has a significant effect on the response value. Therefore, the quadratic polynomial response should be selected for the analysis of the influencing factors of the electrochemical treatment of azo dye wastewater in the dynamic flow diaphragm system, and the model should be used for subsequent prediction and analysis[25].

Using Design Expert software, the variance analysis results of the fitting equation of amaranth decolorization rate (Table 4) and the evaluation (Table 5) were obtained. At the same time, the multiple quadratic regression equation between the response value and the factor is obtained by data regression analysis, as follows:

$$\text{Amaranth red removal rate} = f(A, B, C) = -248{\cdot}2775 + 6{\cdot}5945 \times A + 37{\cdot}21 \times B + 6{\cdot}2155 \times C - 0{\cdot}151 \times A \times B + 0{\cdot}0005 \times A \times C - 0{\cdot}016 \times B \times C - 0{\cdot}1419 \times A^2 - 3{\cdot}3825 \times B^2 - 0{\cdot}050675 \times C^2 \quad (2)$$

From Table 4, it can be seen that the correlation coefficient R^2 of the model is 0.9952, which can accurately fit the change of 99.52 % response value, and the test error is very small; adjusted R^2 and Predicted R^2 were 0.9890 and 0.9509, respectively. The difference between the two numbers was far less than 0.2, indicating that the correlation between the two was good, and the precision and reliability of the model were good. Similarly, the discrete coefficient CV = 0.4424 %, indicating that the model can well reflect the real data of the test, that is, it has high reliability, so the model meets the requirements of prediction and optimization analysis.

It can be seen from Table 5 that the value of the accompanying probability P is less than 0.05, which indicates that it is statistically significant at the 95 % confidence level and has high significance. Therefore, in this model, A, B, C, AB, A^2, B^2, C^2 have high significance, and the order of the influence of three different factors on the removal rate of amaranth can be obtained from the value of F: electrode voltage > cycle speed > plate spacing. At the same time, it can be seen from the table that the accompanying probability P values of AC and BC in the quadratic polynomial regression equation (Formula 3) are all greater than 0.05, which is not significant, so it should be eliminated.

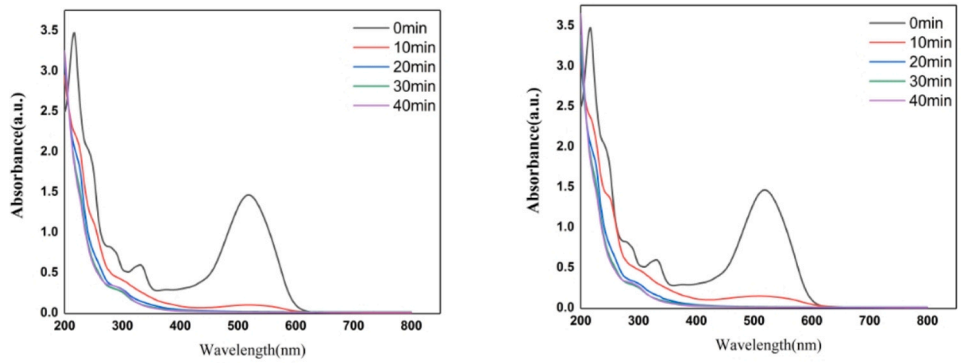

Fig. 12. UV–vis spectrum curve of treated amaranth red dye.

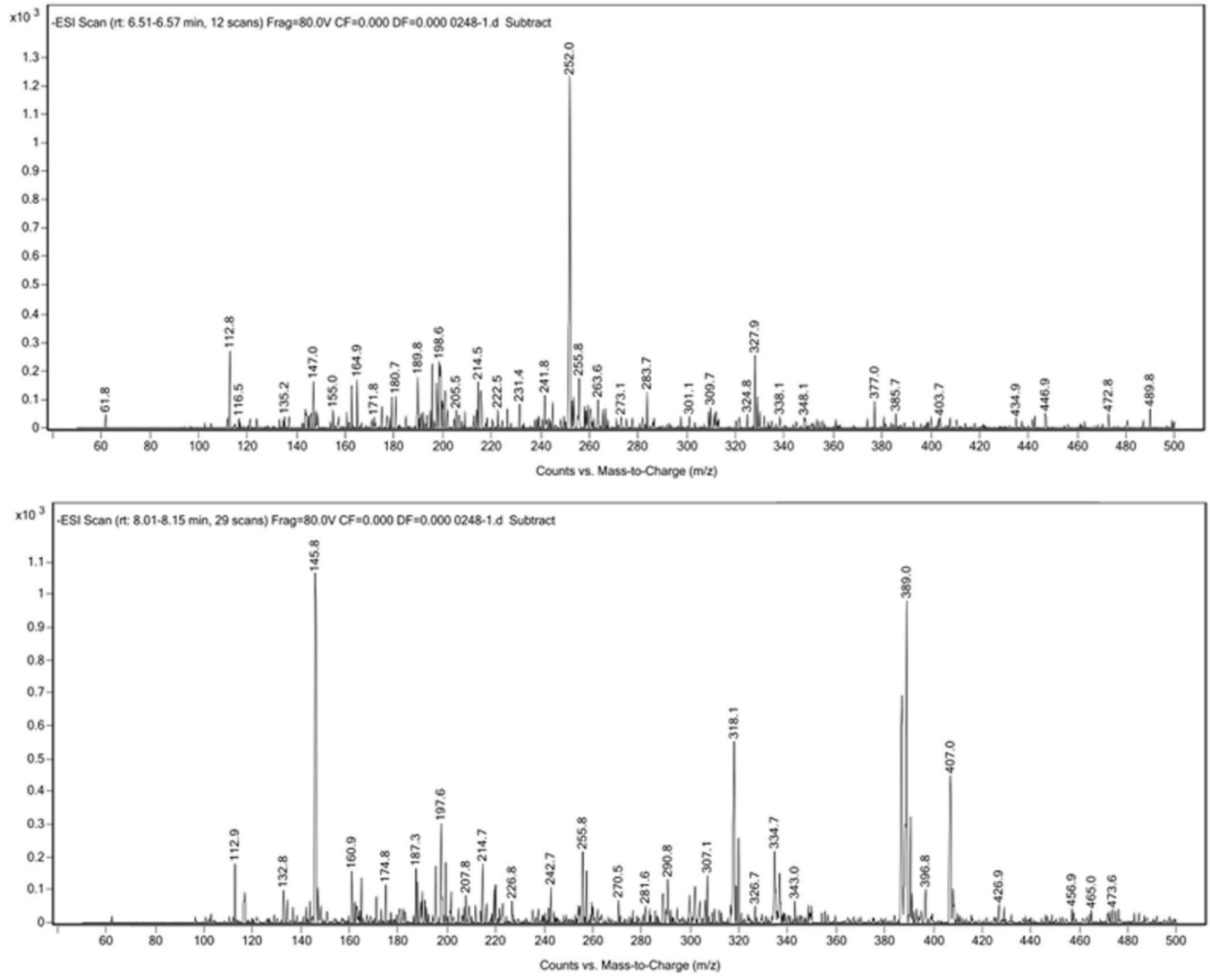

Fig. 13. The mass spectrum of amaranth after electrolysis for 20 min in negative ion mode.

The quadratic polynomial regression equation that converts Equation (Formula 3) into a real independent variable is:

$$\text{Decolorization rate of amaranth red} = -248{\cdot}27750 + 6{\cdot}5945 \times A + 37{\cdot}21 \times B + 6{\cdot}2155 \times C\text{-}0{\cdot}151 \times A\text{-}0{\cdot}1419 \times A^2\text{-}3{\cdot}3852 \times B^2\text{-} 0{\cdot}050675 \times C^2 \quad (3)$$

3.2.3. Two-factor interaction analysis

In order to further explore the interaction between various influencing factors and determine the optimal point, the contour line and three-dimensional response surface diagram of the two-factor interaction were obtained by software analysis. The graph can not only make

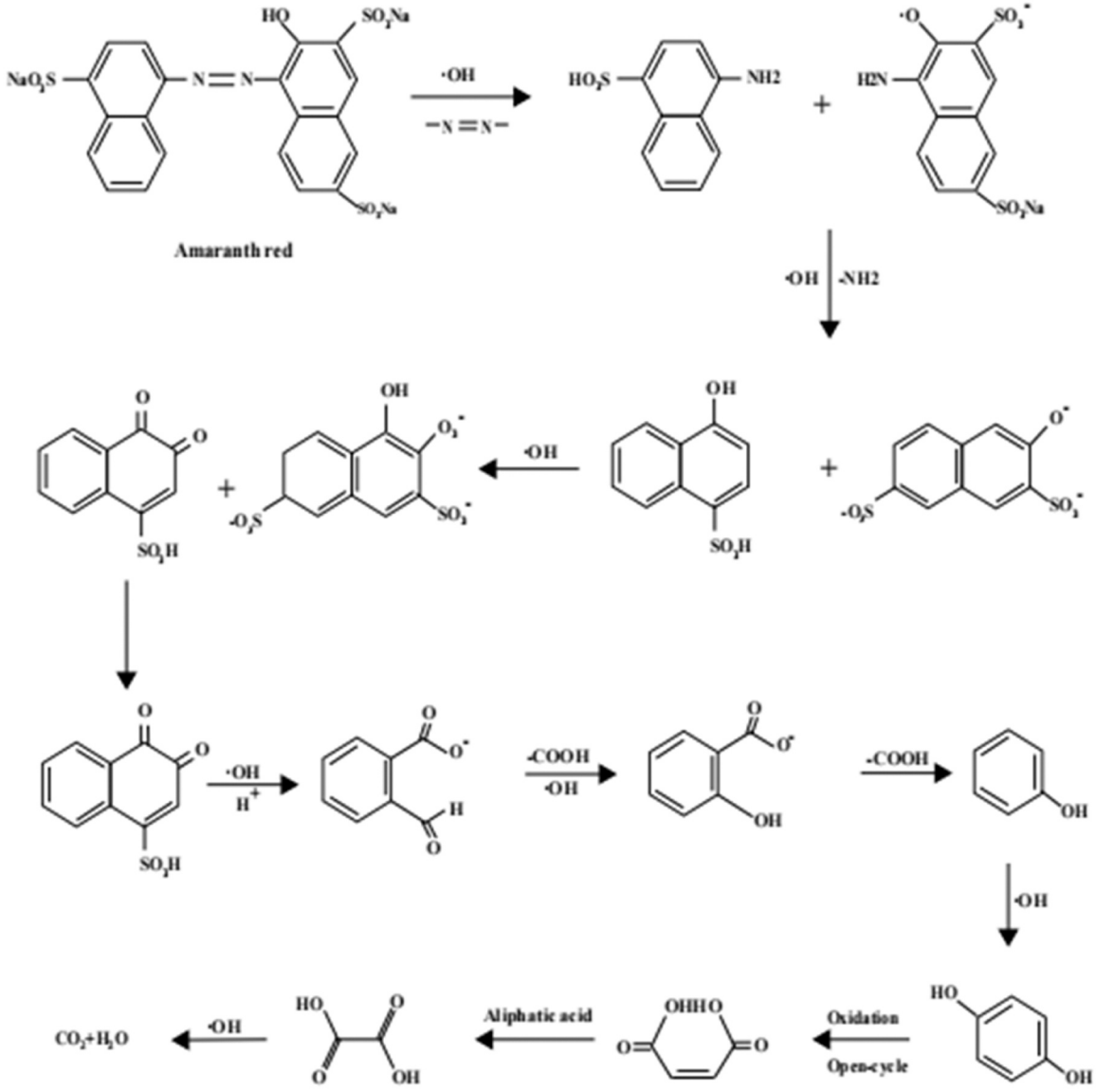

Fig. 14. Schematic representation of the amaranth red removal pathway.

the response value of each point more intuitive, but also analyze the influence relationship between various factors. In the contour map, if the central figure is elliptical, it indicates that the interaction between the two factors is obvious; if the shape is close to a circle, it indicates that the interaction between the two factors is weak. In the response surface diagram, the size of the response value can be judged according to the depth of the color, and the removal effect can be further determined.

From Fig. 6-Fig. 8, the interaction between various influencing factors can be seen intuitively, and the optimal point of amaranth dye removal effect is determined. The optimal response value output by the software is 99.6643 %, that is, when the voltage is 20.7412 V, the plate spacing is 4.89443 cm, and the cycle speed is 60.6583 rad / min, the reaction The removal rate of amaranth dye is 99.6643 %, and the feasibility reaches 96.90 %.

3.3. Analysis and comparison of electrochemical energy consumption

In the actual wastewater treatment process, not only good removal effect but also equipment operation cost need to be saved, so the comparative study of energy consumption is very important. The mathematical energy consumption model of different systems was established by calculating the experimental data, and the relationship between energy consumption and decolorization rate in the degradation and decolorization process of amaranth dye in different systems was analyzed. The circulating diaphragm system uses a peristaltic pump to circulate part of the reaction solution of the two polar chambers, giving full play to the role of the anode and cathode chambers. The two polar chambers of the static diaphragm system react separately and do not affect each other.

3.3.1. Electrochemical energy consumption analysis of static flow separator system

The current value of the static flow diaphragm system under different voltages and the decolorization rate of amaranth dye in the cathode and anode chambers are shown in Table 6, and the relationship curve is shown in Fig. 9. The relationship between voltage and current was analyzed by regression analysis. The regression equation is as follows:

$$I = 0{\cdot}0356\,U + 0{\cdot}262\ ,\ R^2 = 0{\cdot}9966 \tag{4}$$

Decolorization rate of anode chamber:

$$E_1 = 1{\cdot}9652\,U + 67{\cdot}402\ ,\ R^2 = 0{\cdot}9967 \tag{5}$$

Decolorization rate of cathode chamber:

$$E_2 = 1{\cdot}6168\,U + 26{\cdot}18\ ,\ R^2 = 0{\cdot}9963 \quad (6)$$

The calculation formula of the power consumption of the reaction system is as follows:

$$W = UIt \quad (7)$$

The relationship between energy consumption and decolorization rate in anode chamber is as follows:

$$W_1 = (0{\cdot}0092E1^2\text{-}1{\cdot}1093E1 + 32{\cdot}8916)\ t \quad (8)$$

The relationship between energy consumption and decolorization rate in cathode chamber is as follows:

$$W_2 = (0{\cdot}0136E2^2\text{-}0{\cdot}5510E2 + 5{\cdot}0918)\ t \quad (9)$$

3.3.2. Electrochemical energy consumption analysis of dynamic flow separator system

The current value of the dynamic flow diaphragm system under different voltages and the decolorization rate of amaranth dye in the cathode and anode chambers are shown in Table 7, and the relationship curve is shown in Fig. 10. The relationship between voltage and current was analyzed by regression analysis. The regression equation is as follows:

$$I = 0{\cdot}0536\,U + 0{\cdot}224\ ,\ R^2 = 0{\cdot}9964 \quad (10)$$

Decolorization rate of anode chamber:

$$E_3 = 2{\cdot}4736\,U + 58{\cdot}598\ ,\ R^2 = 0{\cdot}9984 \quad (11)$$

Decolorization rate of cathode chamber:

$$E_4 = 2{\cdot}4356\,U + 56{\cdot}276\ ,\ R^2 = 0{\cdot}9939 \quad (12)$$

The calculation formula of the power consumption of the reaction system is as follows:

$$W = UIt \quad (13)$$

The relationship between energy consumption and decolorization rate in anode chamber is as follows:

$$W_3 = (0{\cdot}0088E5^2\text{-}0{\cdot}9361E5 + 24{\cdot}7731)\ t \quad (14)$$

The relationship between energy consumption and decolorization rate in cathode chamber is as follows:

$$W_4 = (0{\cdot}0090E6^2\text{-}0{\cdot}9250E6 + 23{\cdot}4397)\ t \quad (15)$$

The mathematical energy consumption models of the two systems for the treatment of single azo dye amaranth were established. Based on the same reaction time, t can be set as a constant, and the decolorization rate of amaranth dye in the two systems was used as an independent variable to obtain the corresponding W_1, W_2, W_3, W_4, the energy consumption of the two systems and $W_1 + W_2$, $W_3 + W_4$ and the corresponding energy consumption ratio $(W_1 + W_2) / (W_3 + W_4)$ values are shown in Table 8. The comparison of the energy consumption of the two systems is shown in Fig. 11.

From Table 8 and Fig. 11, it can be seen that the energy consumption of the reaction in the static flow diaphragm electrochemical system and the dynamic flow diaphragm electrochemical system decreases first and then increases with the increase of the decolorization rate. The sum of the energy consumption of the cathode and anode in the static flow diaphragm system is the lowest when the decolorization rate is 40 %. Before the decolorization rate is less than 30 %, the energy consumption of the system is always slightly lower than the sum of the energy consumption of the cathode and anode in the dynamic flow diaphragm system, but the difference is not much; when the decolorization rate reaches 90 %, the value of $(W_1 + W_2) / (W_3 + W_4)$ is only 0.34. It can be seen that the dynamic flow separator system has an absolute advantage in energy consumption when treating azo dye wastewater. Therefore, the dynamic flow separator system is more suitable for the treatment of azo dye wastewater.

3.4. Analysis of degradation mechanism of dynamic diaphragm system

3.4.1. Analysis of the mechanism of electrochemical advanced oxidation

In the electrochemical advanced oxidation system of this study, H_2O in the anode chamber discharges on the anode plate to form adsorbed hydroxyl radicals (MO_X (·OH)) and reacts with oxygen atoms in the anode, and enters the metal oxide lattice to form high-valent titanium oxide MO_{X+1}[26,27]. When organic matter is present in the solution, two reactions of ' electrochemical combustion ' and ' electrochemical conversion ' occur in the system[28]. In the process of ' electrochemical combustion ', the physical adsorption of reactive oxygen species plays a major role, but in the process of ' electrochemical conversion ', the chemical adsorption of reactive oxygen species plays a major role. The main reactions are as follows, where R represents organic pollutants:

$$MO_X + H_2O \rightarrow MO_X(\cdot OH) + H^+ + e^- \quad (16)$$

$$MO_X(\cdot OH) \rightarrow MO_{X+1} + H^+ + e^- \quad (17)$$

$$MO_{X+1} \rightarrow O_2 + MO_X \quad (18)$$

$$R + MO_X(\cdot OH)_Y \rightarrow CO_2 + MO_{X+Y} + H^+ + Ye^- \quad (19)$$

$$R + MO_{X+1} \rightarrow RO + MO_X \quad (20)$$

3.4.2. Analysis of molecular removal mechanism of azo dyes

Fig. 12 (a) and (b) show the UV-Vis spectra of amaranth dye at different reaction time when the anode and cathode degrade the amaranth dye respectively. It can be seen from the figure that several main characteristic peaks of amaranth dye are 217 nm, 238 nm, 280 nm, 330 nm, and the maximum absorption wavelength is 521 nm. The peak at 280 nm and 330 nm is the characteristic peak of naphthalene ring structure, which is caused by the π-π * transition of benzene ring conjugated system. The main color group of amaranth dye molecule is at 521 nm, and the peak is mainly caused by the n-π * transition of the azo structure. The absorption peaks of the anode and cathode gradually weakened with the reaction. After 40 min of the reaction, all kinds of absorption peaks basically disappeared, indicating that the naphthalene ring and azo structure in the amaranth dye were destroyed, the chromophore disappeared, and the decolorization effect was achieved.

As shown in Fig. 13, the intermediate products of the interpretation process were qualitatively identified by LC-MS analysis of amaranth solution after 20 min of treatment.

In short, during the reaction of the system, the amaranth dye is mainly oxidized by the oxidizing substances produced by the anode, destroys its N = N double bond, and forms a nitroaromatic compound. The nitroaromatic compound is sent to the cathode for reduction by cyclic action, and the nitro group on the benzene ring is reduced and replaced, and converted into an amine group and a hydroxyl group. Further oxidation causes the naphthalene ring and the benzene ring to react and break to form a small molecule substance, and finally generate CO_2, H_2O [29,30]. Combined with the research and analysis results of other scholars on azo dyes[31–33], the degradation process of amaranth dye in dynamic flow was deduced, and the results are shown in Fig. 14.

4. Conclusion

This experiment provides a reference for the treatment of azo dye wastewater.

1. After optimizing the single factor by response surface method, the optimal reaction conditions were obtained. When the voltage is 20.74 V, the plate spacing is 4.89 cm, and the cycle speed is

60.66 rad / min, the best response value of degradation is 99.66 %, and the feasibility is 96.9 %.
2. The energy consumption of dynamic flow diaphragm system and static flow diaphragm system is analyzed. When the decolorization rate of amaranth dye reaches 90 %, the energy consumption of the cathode and anode chambers of the dynamic flow diaphragm system is 34 % of that of the static flow diaphragm system, which verifies that the electrochemical method of the dynamic flow diaphragm system has more advantages in the treatment of azo dye wastewater.
3. After oxidative degradation, amaranth was finally converted into harmless small molecules and water, and the possible degradation path of azo dye wastewater by dynamic flow membrane system was inferred by UV–vis spectroscopy and LC-MS analysis.

The results show that the dynamic flow membrane system process has great potential in the treatment of azo dye wastewater, and provides a new and efficient treatment scheme for dye wastewater treatment.

Author contributions

In this research work, Ao Xiao and Fuchen Ban participated in the design and operation of experiments and the preparation of papers, and Xiaoyi Tong was responsible for a proofreading and theoretical derivation; Chenjian Ye and Yu Wei assisted and measured the experimental operation. All authors agree on the final version of the paper.

CRediT authorship contribution statement

Ao Xiao: Writing – review & editing, Writing – original draft, Visualization, Validation, Methodology, Investigation, Funding acquisition, Formal analysis, Data curation, Conceptualization. **Fuchen Ban:** Writing – review & editing, Writing – original draft, Methodology, Funding acquisition, Formal analysis, Data curation, Conceptualization. **Xiaoyi Tong:** Methodology, Formal analysis, Data curation. **Yu Wei:** Methodology. **Chenjian Ye:** Resources, Formal analysis.

Data Availability

The authors do not have permission to share data.

Declaration of Competing Interest

The authors declare that they have no known competing financial interests or personal relationships that could have appeared to influence the work reported in this paper.

Acknowledgements

This study was supported by the National Water Pollution and Control Major Project: Simulation and verification of key and integrated technologies for water pollution control in Liaohe River Basin (2018ZX07601001-3).

References

[1] Anjaneya O, Shrishailnath SS, Guruprasad K, Nayak AS, Mashetty SB, Karegoudar TB. Int Biodeterior Biodegrad 2013;79:64–72.
[2] Singh R, Singh R, Singh P. Toxicol Int 2014;21.
[3] Ooi J, Lee LY, Hiew BYZ, Thangalazhy-Gopakumar S, Lim SS, Gan S. Bioresour Technol 2017;245:656–64.
[4] Basu A, Suresh Kumar G. J Agric Food Chem 2014;62:7955–62.
[5] Alarcón M, Jarro RYA, Ahmed MA, Bustos KAG, Tanaka DAP, Hilares RT. Ultrason Sonochem 2022;89:7.
[6] Adekunle ASO, Durosinmi JAO, Saheed LM, Ajayeoba O, Akinyele TA, Elugoke OF, Oluwafemi SE, O. S. Nano-Struct Nano-Objects 2021:*28*.
[7] Guo M, Yuan B, Sui Y, Xiao Y, Dong J, Yang L, Bai L, Yang H, Wei D, Wang W, Chen H. J Colloid Interface Sci 2023;631:33–43.
[8] Castro FD, Bassin JP, Dezotti M. Environ Sci Pollut Res 2017;24:6307–16.
[9] Chaturvedi A, Jaiswal RP. Environ Sci Pollut Res 2022;29:88018–26.
[10] Miklos DB, Remy C, Jekel M, Linden KG, Drewes JE, Hübner U. Water Res 2018;139:118–31.
[11] Cotillas S, Llanos J, Cañizares P, Clematis D, Cerisola G, Rodrigo MA, Panizza M. Electrochim Acta 2018;263:1–7.
[12] Jiao Y, Ma L, Tian Y, Zhou M. Chemosphere 2020;252.
[13] Panizza M, Delucchi M, Cerisola G. J Appl Electrochem 2005;35:357–61.
[14] Shi JH, Gong L, Zhang T, Sun SY. Membranes 2022;12:11.
[15] Alkhadra MA, Gao T, Conforti KM, Tian HH, Bazant MZ. Desalination 2020;476:8.
[16] Nemati M, Hosseini SM, Shabanian M. J Hazard Mater 2017;337:90–104.
[17] Zlotorowicz A, Strand RV, Burheim OS, Wilhelmsen O, Kjelstrup S. J Membr Sci 2017;523:402–8.
[18] Hu Y, Mao XH, Cui JX, Xiong LL, Yin PJ, Zhou SB, Wang X. Chemistryselect 2019;4:5064–72.
[19] Ma XJ, Zhou MH. J Chem Technol Biotechnol 2009;84:1544–9.
[20] Shokoufi N, Shemirani F, Assadi Y. Anal Chim Acta 2007;597:349–56.
[21] Xiong Y, He C, Karlsson HT, Zhu XH. Chemosphere 2003;50:131–6.
[22] Pan G, Jing X, Ding X, Shen Y, Xu S, Miao W. J Alloy Compd 2019;809:151749.
[23] Palma-Goyes RE, Silva-Agredo J, González I, Torres-Palma RA. Electrochim Acta 2014;140:427–33.
[24] Abdelwahab O, Amin NK, El-Ashtoukhy ESZ. J Hazard Mater 2009;163:711–6.
[25] Wang HP, Wang B, Peng Y, Crittenden JC, Pan HF, Wang LX. Environ Sci-Water Res Technol 2022;9:308–30.
[26] Panizza M, Cerisola G. Chem Rev 2009;109:6541–69.
[27] Zoellig H, Fritzsche C, Morgenroth E, Udert KM. Water Res 2015;69:284–94.
[28] Yao Y, Chen Q, Zhou J. Int J Environ Sci Technol 2021;19:1799–810.
[29] Roşu M-C, Socaci C, Floare-Avram V, Borodi G, Pogăcean F, Coroş M, Măgeruşan L, Pruneanu S. Mater Chem Phys 2016;179:232–41.
[30] Steter JR, Barros WRP, Lanza MRV, Motheo AJ. Chemosphere 2014;117:200–7.
[31] Konstantinou IK, Albanis TA. Appl Catal B: Environ 2004;49:1–14.
[32] López C, Valade A-G, Combourieu B, Mielgo I, Bouchon B, Lema JM. Anal Biochem 2004;335:135–49.
[33] Bansal P, Singh D, Sud D. Sep Purif Technol 2010;72:357–65.